CHEMISTRY
A EUROPEAN JOURNAL

DOI: 10.1002/chem.200901601

Correlation of the Catalytic Activity for Oxidation Taking Place on Various TiO_2 Surfaces with Surface OH Groups and Surface Oxygen Vacancies

Zhanfeng Zheng,[a] Jaclyn Teo,[b] Xi Chen,[a] Hongwei Liu,[a] Yong Yuan,[a] Eric R. Waclawik,[a] Ziyi Zhong,*[b] and Huaiyong Zhu*[a]

Abstract: Three catalytic oxidation reactions have been studied: The ultraviolet (UV) light induced photocatalytic decomposition of the synthetic dye sulforhodamine B (SRB) in the presence of TiO_2 nanostructures in water, together with two reactions employing Au/TiO_2 nanostructure catalysts, namely, CO oxidation in air and the decomposition of formaldehyde under visible light irradiation. Four kinds of TiO_2 nanotubes and nanorods with different phases and compositions were prepared for this study, and gold nanoparticle (Au-NP) catalysts were supported on some of these TiO_2 nanostructures (to form Au/TiO_2 catalysts). FTIR emission spectroscopy (IES) measurements provided evidence that the order of the surface OH regeneration ability of the four types of TiO_2 nanostructures studied gave the same trend as the catalytic activities of the TiO_2 nanostructures or their respective Au/TiO_2 catalysts for the three oxidation reactions. Both IES and X-ray photoelectron spectroscopy (XPS) proved that anatase TiO_2 had the strongest OH regeneration ability among the four types of TiO_2 phases or compositions. Based on these results, a model for the surface OH group generation, absorption, and activation of molecular oxygen has been proposed: The oxygen vacancies at the bridging O^{2-} sites on TiO_2 surfaces dissociatively absorb water molecules to form OH groups that facilitate adsorption and activation of O_2 molecules in nearby oxygen vacancies by lowering the absorption energy of molecular O_2. A new mechanism for the photocatalytic formaldehyde decomposition with the Au/TiO_2 catalysts is also proposed, based on the photocatalytic activity of the Au-NPs under visible light. The Au-NPs absorb the light owing to the surface plasmon resonance effect and mediate the electron transfers that the reaction needs.

Keywords: adsorption · catalytic oxidation · gold · surface chemistry · TiO_2

Introduction

TiO_2 is the most extensively studied photocatalyst for the decomposition of organic pollutants in water and air owing to its high efficiency, stability, nontoxicity, and low cost.[1,2] It is also used to support heterogeneous gold catalysts for catalytic oxidation reactions of HCHO[3,4] and CO.[5–7] In these catalytic oxidation reactions with molecular O_2 as the oxidant, O_2 activation is the key step. Therefore, to understand the catalytic origin of these oxidation reactions and to design efficient catalysts, it is essential to know the activation route of molecular O_2 on the catalyst surfaces. Recently, a scanning tunneling electron microscopy (STM) study performed in a ultrahigh vacuum provided evidence that molecular O_2 is adsorbed on the defects on the (110) surface of a rutile single crystal, and that the oxygen diffusion rate was dependent on the surface oxygen vacancy density.[8] However, it is still a challenge to acquire such information on the TiO_2 surface or on supported Au/TiO_2 catalysts accurately under typical reaction conditions. In the case of supported gold catalysts, because gold species in high oxidation states are usually not stable and their oxidation state changes easily, the associated active oxygen species are not easy to identify.[9]

[a] Dr. Z. Zheng, Dr. X. Chen, Dr. H. Liu, Dr. Y. Yuan, Dr. E. R. Waclawik, Prof. Dr. H. Zhu
School of Physical and Chemical Sciences
Queensland University of Technology
GPO Box 2434, Brisbane, Qld 4001 (Australia)
Fax: (+61) 07 31381804
E-mail: hy.zhu@qut.edu.au

[b] J. Teo, Dr. Z. Zhong
Institute of Chemical Engineering and Sciences
Agency for Science Technology and Research (A-Star)
1 Pesek Road, Jurong Island, 627833 (Singapore)
Fax: (+65) 6316 6182
E-mail: zhong_ziyi@ices.a-star.edu.sg

Supporting information for this article is available on the WWW under http://dx.doi.org/10.1002/chem.200901601.

For supported gold catalysts that are used for CO oxidation, the catalyst supports have three roles: 1) to support the active gold particles mechanically, 2) to modify the electronic properties of the gold particles, and 3) to mediate oxygen supply in the reaction. Usually, reducible catalyst supports such as TiO_2 are categorized as active catalyst supports. Although the reducibility of the supports is one of the requirements for a high catalytic activity, it cannot explain the observation that CO oxidation can take place at a temperature much lower than that of the reduction temperature of the support.[9] In addition, it has been experimentally proven that moisture also plays an essential role in low-temperature CO oxidation on supported gold catalysts by contributing to the formation and regeneration of the surface active sites.[10,11] Haruta et al. later reported that this effect of the moisture is dependent on the catalyst support.[10,12] However, so far a detailed mechanism that involves the role of moisture and that of catalyst supports has not been well addressed.

Because of the extensive studies on the photocatalytic water-splitting reaction on TiO_2 surfaces,[13] it is well known that water molecules can either dissociate at oxygen vacancies (defects) on the TiO_2 surface to yield surface OH groups, or physically adsorb on these sites. These physically adsorbed and dissociated H_2O molecules can be monitored by measuring the infrared (IR) spectra of the samples.[7,14,15] On the other hand, theoretical studies have revealed that surface OH groups on TiO_2 can facilitate adsorption and activation of molecular oxygen.[16,17] In a recent coupled thermogravimetric–FTIR (TG–FTIR) study on an Au/α-Fe_2O_3 catalysts for CO oxidation,[18] it was proven that at low temperatures, small gold nanoparticles (Au-NPs) cannot activate the oxygen of the support lattice directly, and thus the lattice oxygen does not participate in the reaction, but instead, it is molecular oxygen species that are responsible for the low-temperature CO oxidation. Some theoretic calculations have shown that adsorption of O_2 on isolated Au clusters requires an unpaired electron from the metal particle, and preferably an anionic Au species, leading to the formation of superoxo or peroxy anions. However, dissociative adsorption of O_2 has a kinetic barrier higher than that for O_2 desorption.[19] Bokhoven et al.[20] studied the Au/Al_2O_3 catalyst by in situ high-energy-resolution and time-resolved X-ray spectroscopy techniques and believed that reduced Au particles could transfer charge to oxygen and activate it. However, Kung et al. believed there was only a very small quantity of adsorbed oxygen on the Au species in a Au/TiO_2 catalyst.[21] Meanwhile, there are a lot of reports showing that the activation of molecular O_2 mainly occurs on the catalyst support,[9,10,22] and as discussed above, are probably related to the surface OH groups and to the surface oxygen vacancy concentration and distribution. Based on this knowledge, a logical hypothesis could be proposed in which the defect sites on the TiO_2 surfaces may play a key role in the catalytic oxidations by using molecular O_2 as oxidant, and that the enhanced O_2 and H_2O adsorption due to these defects results in increased activity. This hypothesis could be verified by correlating the IR bands corresponding to the surface OH groups and physically adsorbed water on the surface defects with the catalytic activity for oxidation taking place on the TiO_2 surface. To conduct such a study, a series of TiO_2 surfaces with large specific surface areas must be employed to enable observation of clear differences in the IR bands and in catalytic activity.

Au-NPs have also been doped on to TiO_2 photocatalysts to enhance their performance for photocatalytic oxidation of organic molecules,[23–25] but the role of the Au-NPs has not been correctly understood. The surface plasmon resonance effect of Au-NPs, which is responsible for the visible light absorption by the Au-NPs, has been recognized for years, and recently we have found that the Au-NPs themselves exhibit significant photocatalytic activity under visible light irradiation.[4] Such activity should be taken into account when interpreting the mechanism of the photocatalytic oxidation with Au-NPs supported on TiO_2 solids.

In this study, four types of TiO_2 nanostructured solids (NTM, a metastable phase between a hydrogen titanate and a TiO_2(B) phase (a monoclinic polymorph of titanium dioxide); NTMA, a thin anatase-layer covered metastable phase; NTB, a mixed TiO_2(B) and anatase phase; and NTA, an anatase phase) were prepared and deposited in the presence of gold to yield four Au/TiO_2 (3 wt%) catalysts. The Au/TiO_2 catalysts were used for the photocatalytic oxidation of HCHO in air at 20°C under blue light (with wavelength between 400 and 500 nm) and for CO oxidation at moderate temperatures in the gas phase. The bare TiO_2 nanostructured solids were also directly used as photocatalysts in the oxidation of the dye sulforhodamine B (SRB) in aqueous solution under ultraviolet (UV) irradiation. The three oxidation reactions have a common feature of using molecular O_2 as the oxidant. We found that the catalytic activities for all three reactions gave the same trend as the order of the surface OH group regeneration ability of the TiO_2 nanostructures that was observed by using FTIR emission spectroscopy (IES).

Results and Discussion

Characterization of the TiO_2 nanostructured solids and gold particles: By indexing the diffraction peaks of the XRD patterns in Figure 1, the NTM sample was found to consist of the metastable phase, the NTMA sample consisted of the mixed metastable and anatase phases, the NTBA sample consisted of the mixed TiO_2(B) and anatase phases, and the NTA sample consisted of the anatase phase. To verify the structure of NTMA further, Raman spectra were also measured for the hydrogen titanate sample before and after the acid-treated sample at 60°C (see Figure S1 in the Supporting Information). The bands at 448 and 663 cm^{-1} were assigned to Ti-O-Ti vibrations, which are found in both hydrogen titanate and acid-treated hydrogen titanate nanotubes. The band at 152 cm^{-1} was only observed in the spectrum of the acid-treated hydrogen titanate nanotubes, and was as-

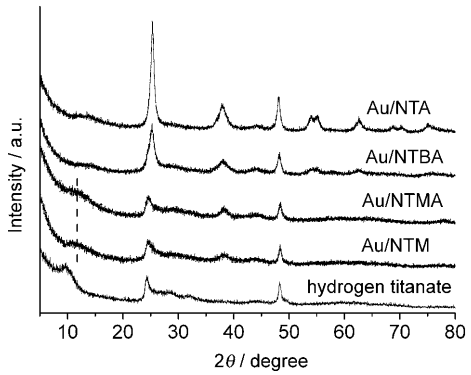

Figure 1. XRD patterns of Au/TiO_2 (3 wt %) nanostructured catalysts.

signed to the anatase A_{1g} vibrational mode.[26] The Raman results confirmed that the NTMA nanotubes consisted of hydrogen titanate and anatase phases. The XRD patterns in Figure 1 also indicated that loading with Au-NPs and subsequent calcination at 300 °C did not cause any phase change in the nanotube supports. According to the Brunauer–Emmett–Teller (BET) results in Table 1, the TiO_2 nanostructures possessed large specific surface areas, so changes in the surface properties could clearly be observed. This property is ideal for the IES studies.

The morphology and structure of the Au-NPs was determined from high-resolution transmission electron micrographs (HRTEM, Figure 2). The Au-NPs were spherical and the Au (111) plane was observed in the HRTEM images of all the gold catalysts. The transmission electron microscopy (TEM) results (Figure 3) showed that the Au-NPs in all of the catalysts were similar. More than 80 % of the Au-NPs were prepared in the size range 4–8 nm (an average obtained from the measurement of 100 Au-NPs) from a series of HRTEM and TEM images. The large specific surface area of these supports allowed the effective dispersion of the Au-NPs. Moreover, X-ray photoelectron spectroscopy (XPS) analysis of the supported Au-NPs (Figure 5) indicated that the gold was present in the metallic state in all of the samples (with the Au $4f_{7/2}$ and Au $4f_{5/2}$ peak identified at 83 eV and 86.5 eV, respectively).

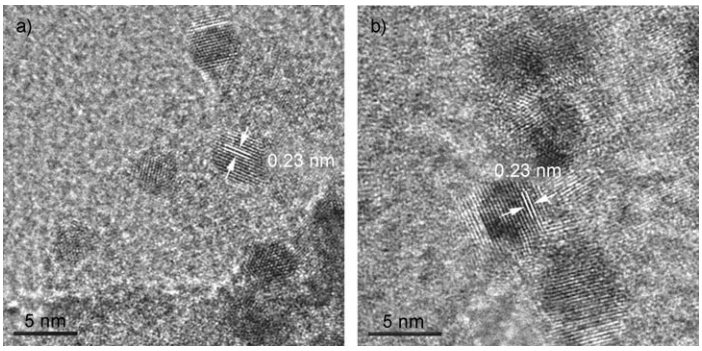

Figure 2. HRTEM images of Au-NPs for a) Au/NTM and b) Au/NTA catalysts.

Results of the IES measurements: The IES technique was employed to investigate water adsorption and dissociation. It was also used to elucidate the defects on the TiO_2 nanostructure surfaces from the IES bands and their changes in conjunction with information acquired from the TEM observations. The IES spectra of the TiO_2 samples are shown in Figure 4. During the IES measurement, the spectra were recorded in situ when the sample was heated on a sample holder from 100 to 300 °C at intervals of 50 °C in a N_2 flow. Because all of the TiO_2 nanostuctures were obtained after calcination at 300 °C or above for 3 h, they were stable during the measurement (i.e., no phase transition took place).

As can be seen, two OH stretching bands at 3705 and 3665 cm^{-1} were observed for all of the samples. The band at 3665 cm^{-1} was assigned to hydrogen bonded (adjacent) OH groups, whereas the band at 3705 cm^{-1} was assigned to isolated OH groups.[27] The intensity of the band at 3665 cm^{-1} considerably decreased when the samples were heated from 100 to 300 °C, whereas that of the band at 3705 cm^{-1} only slightly changed. Clearly, the isolated OH groups were more difficult to remove from the surface than the adjacent OH groups by the heating treatment. At 300 °C (Figure 4, traces d), the band intensity of the adjacent OH groups decreased to a level similar to that of the isolated OH groups. It was also found that the band at 1620 cm^{-1} (H-O-H bending vibrations, not shown in Figure 4) varied harmoniously with the broad band between 3000–3500 cm^{-1} (Figure 4). In the IES spectra, the band at approximately 3400 cm^{-1} is attributed to the hydrogen-bound surface OH groups (Ti–OH) stretching vibration (hydrogen bonded with water molecules), whereas the band at 3250 cm^{-1} is attributed to the stretching vibration of the water molecules that are hydro-

Table 1. Catalytic performance of TiO_2 nanostructures and Au/TiO_2 nanostructure catalysts.

Catalyst	S_{BET}[a] [$m^2 g$]	SRB oxidation[b]		Catalyst	CO oxidation[c]		HCHO oxidation[d]	
		Conversion [%]	TOF [s^{-1}]		Conversion [%]	TOF [s^{-1}]	Conversion [%]	TOF [s^{-1}]
NTM	294.6	15.84	8.4×10^{-8}	Au/NTM	5.38	5.2×10^{-2}	20.55	4.1×10^{-4}
NTMA	306.6	21.07	1.1×10^{-7}	Au/NTMA	15.86	1.5×10^{-1}	32.51	6.5×10^{-4}
NTBA	236.7	30.32	1.6×10^{-7}	Au/NTBA	38.89	3.7×10^{-1}	67.17	1.3×10^{-3}
NTA	192.7	42.44	2.3×10^{-7}	Au/NTA	55.67	5.4×10^{-1}	87.47	1.7×10^{-3}

[a] S_{BET} = Specific surface area determined by BET analysis. [b] SRB oxidation conversion was calculated after reacting for 90 min with the SRB (C_0) and catalyst concentration of 1.8×10^{-5} mol L^{-1} and 0.5 g L^{-1}, respectively. [c] CO oxidation was performed at 30 °C under 197 mL min^{-1} CO (1 %) flow in the presence of the catalyst (10 mg). [d] HCHO oxidation was performed at 20 °C for 120 min in the presence of HCHO (4 μL, liquid injection) and catalyst (20 mg).

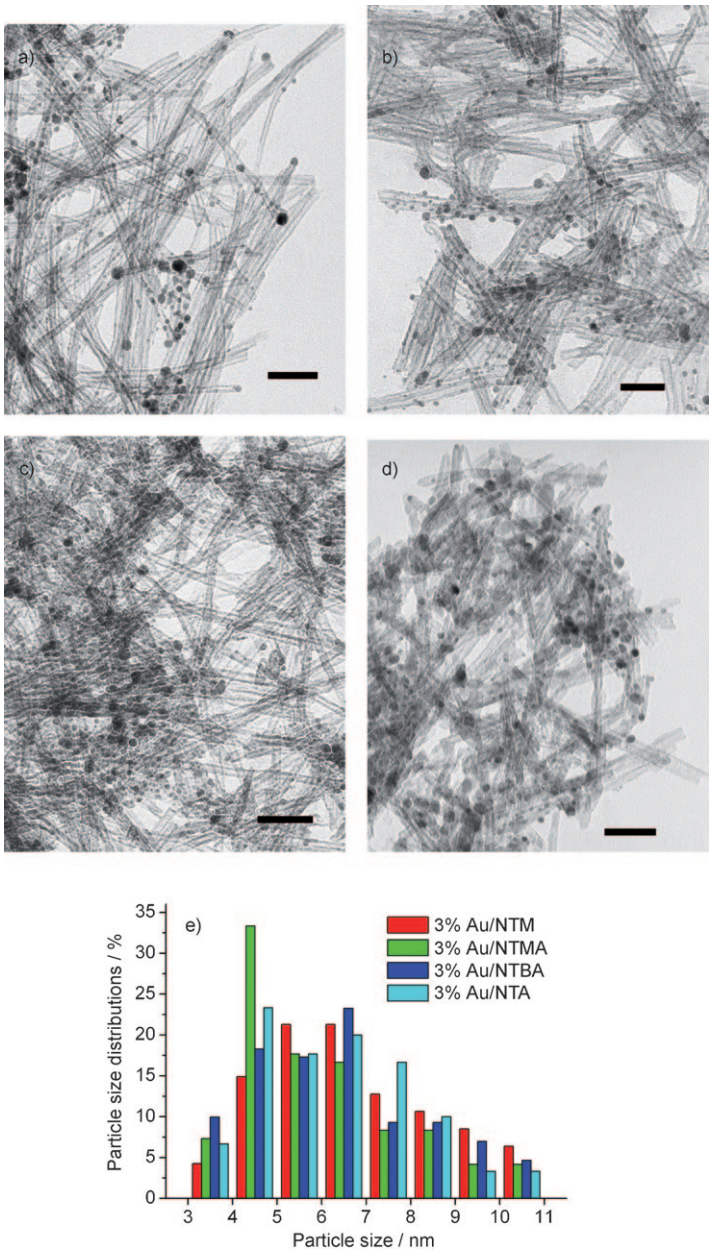

Figure 3. TEM images of Au (3 wt%) supported on various TiO_2 nanostructured substrates: a) Au/NTM, b) Au/NTMA, c) Au/NTBA, d) Au/NTA catalysts, and e) the distribution of Au-NPs. The scale bars are all 50 nm. The particle size distributions were determined by analyzing 100 Au-NPs by using HRTEM images taken from several specimens.

gen bonded.[14,15] When heated to above 150 °C, the band at approximately 3250 cm^{-1} weakened and the band at approximately 3400 cm^{-1} became visible, indicating that the absorbed water could be readily removed. The band at 1620 cm^{-1} completely disappeared when the samples were heated in situ at 300 °C in a flow of N_2, together with those at approximately 3400 cm^{-1} for the hydrogen-bonded OH group and water. Loss of the surface OH groups and absorbed water is easier on NTM than on NTA in our IES measurements, whereas in the cooling process (just after the heating at 300 °C), these bands reappeared in the spectra of both NTM and NTA, but the reappearance was observed at a lower temperature in the spectra of NTM. When the temperature was lowered to 150 °C, the band at 3665 cm^{-1} for NTA was regenerated with much higher intensity than that of NTM. This is clear proof that the NTA surface has a stronger ability to adsorb and dissociate water (rehydoxylation). The water molecules that were present were probably due to the trace moisture in the N_2 flow or diffusion from atmosphere because the IES system is not completely isolated from air. The recovery of the absorbed water (the broad band at 3000–3500 cm^{-1} and the band at 1620 cm^{-1}) was clearly seen when the temperature was decreased to 100 °C. Similar to rehydoxylation, an intensive band due to the reabsorbed water was observed for the NTA sample, and it was a stronger band than for NTM sample (Figure 4, traces f). When the N_2 flow was shut off and the specimen was exposed to air at 100 °C for 10 min, the intensity of the same band was almost fully recovered for the NTA sample but was only partially recovered for the NTM sample. According to the IES results, the ability of the TiO_2 nanostructures to regain surface OH groups and absorbed water is in the order NTA > NTBA > NTMA > NTM.

It should be emphasized that, because the IES measurements for all of the samples were carried out under the same conditions (N_2 flow rate and heating and cooling procedures), the measured IES spectrum for a specific sample was well reproducible. Moreover, the same order was observed for the TiO_2 nanostructures loaded with gold (results not shown here), confirming that the rehydroxylation and re-adsorption of water took place on the TiO_2 support surface.

Results of the XPS measurements: The discovery that the NTA sample had the strongest surface OH group regeneration ability was also confirmed by XPS measurements. Figure 5 shows the O 1s spectra of the Au/TiO_2 (NTA) and Au/TiO_2 (NTM) catalysts before and after the CO oxidation reaction (more reaction results are discussed below). The main O 1s peak (either before or after the reaction) is at approximately 530–530.2 eV, revealing the main component of the lattice oxygen (O^{2-}) species in the supports. However, besides the normal lattice oxygen species at 530.2 eV and the surface OH species at approximately 531.8 eV, an interesting O 1s shoulder peak at 534.9 eV was observed, but only in the Au/TiO_2(NTA) catalyst after the reaction. Tabayashi et al.[28] calculated the X-ray spectra of small formic acid clusters by using density functional theory, and predicated that in addition to the normal O 1s binding energy at 532 eV, which is attributed to O 1s (C=O)→π* (C=O) excitation, there would be an additional O 1s peak at 535 eV, originating from three transitions: O 1s (C=O)→σ*(OH), O 1s (OH)→π* (C=O), and O 1s (OH)→σ*(OH). The observation of the O 1s peak at 534.9 eV (Figure 5) indicates the interaction of the CO groups with the OH groups on the surface of the Au/TiO_2 (NTA) catalyst, revealing the strongest OH regeneration ability of the NTA support. This

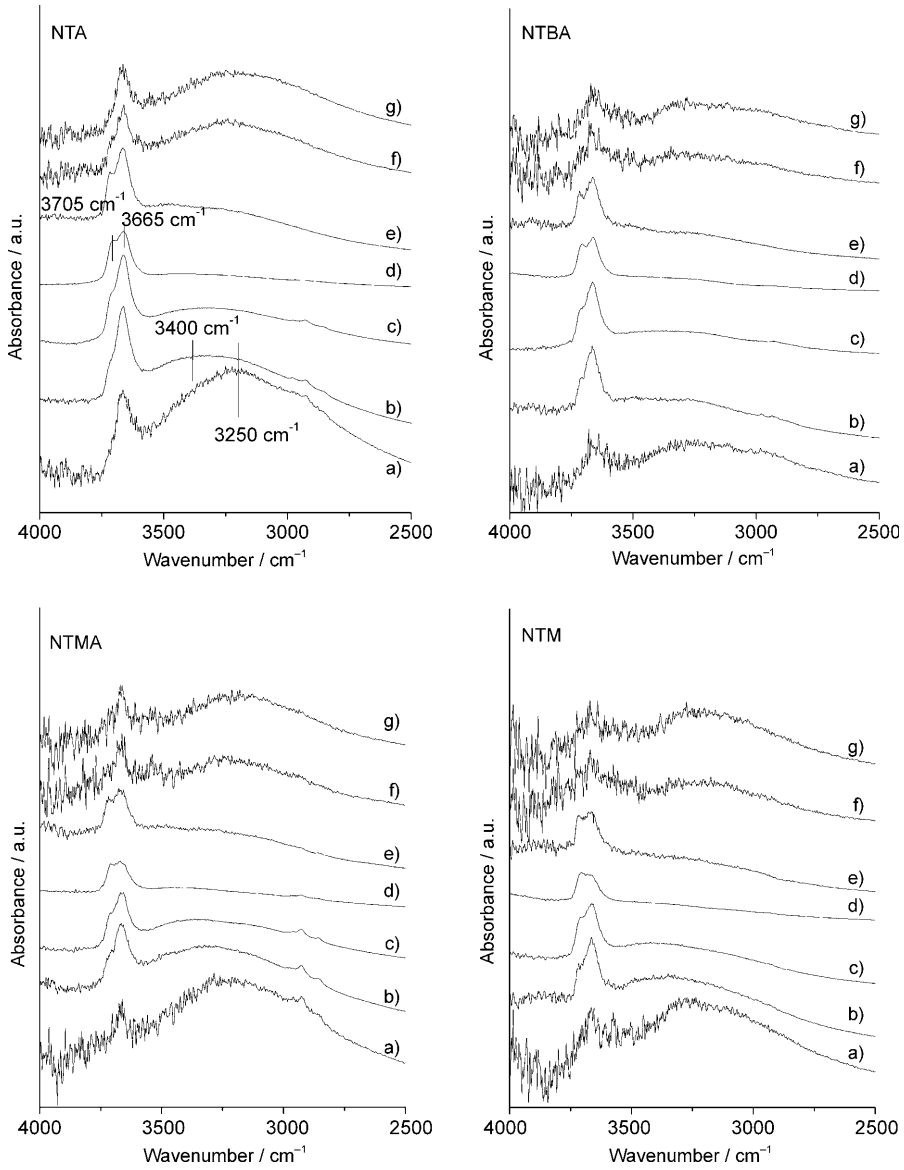

Figure 4. IES spectra of NTA, NTBA, NTMA, and NTM samples. Traces a), b), c), and d), were measured at 100, 150, 200, and 300 °C, respectively; traces e) and f) were obtained after the temperature was lowered from 300 °C to150 and 100 °C, respectively; trace g) was measured when the samples had been exposed to air at 100 °C for 10 min.

CO + OH complex could be formed in the CO oxidation reaction owing to the abundance of OH groups in the NTA supports, or it could be generated after the catalytic reaction during transfer of the sample to the XPS sample chamber (owing to the high surface OH regeneration ability of the NTA support and the fact that the sample was unavoidably exposed to air for a short time during the operation). Similar results were reported by Kung et al.,[21] who observed an IR peak at 1242 cm^{-1}, which was assigned to a hydroxycarbonyl species after an Au/TiO_2 catalyst was exposed to CO gas. Because the NTM sample exhibited the weakest OH regeneration ability among the four TiO_2 samples, it is understandable that a similar O 1s peak at 534.9 eV was not observed in this case.

Catalyst performance results: The surface OH groups could facilitate O_2 absorption, and thus, binding and activation of O_2 could be significantly enhanced in the presence of water.[16,29,30] We found that the catalytic activity of the catalysts for all of the three oxidation reactions strongly depended on the ability of the TiO_2 nanostructures to regain surface hydroxyl groups and absorbed water. Catalyst activity curves are shown in Figure 6 and the catalytic test conditions, conversion, and turnover frequency (TOF) are derived from conversion and the content of the active component of the catalyst, which are listed in Table 1. The TOF for the SRB photocatalytic degradation was calculated based on the total TiO_2 because TiO_2 is the active component of the photocatalysts. The TOF for the other reactions were calculated based on gold content because gold is the active component. Of all of the three reactions the NTA sample and its supported gold catalyst exhibited the highest activity followed by NTBA, NTMA, and NTM and their respective supported gold catalysts.

For the catalysts containing gold, the Au-NPs were loaded onto the supports by using the same procedure. Analysis of TEM and XPS results demonstrated that the Au-NPs in all of the catalyst samples were similar in terms of size (4–8 nm), shape, dispersion, and oxidation state. X-ray fluorescence (XRF) analysis showed that the gold loadings on all of the supports were similar at about 3 wt %. These facts suggest that the difference in the supports has a limited effect on the properties of the Au-NPs in these catalysts. Consequently, the difference in catalytic activities of the catalysts is mainly attributed to the difference in the supports, especially the difference in the surface structures.

Mechanism of photocatalytic HCHO oxidation: For HCHO oxidation under visible light (wavelength of 400–500 nm), all of the photocatalysts of the Au-NPs on TiO_2 supports exhibited significant activity (Table 1). Because the bare sub-

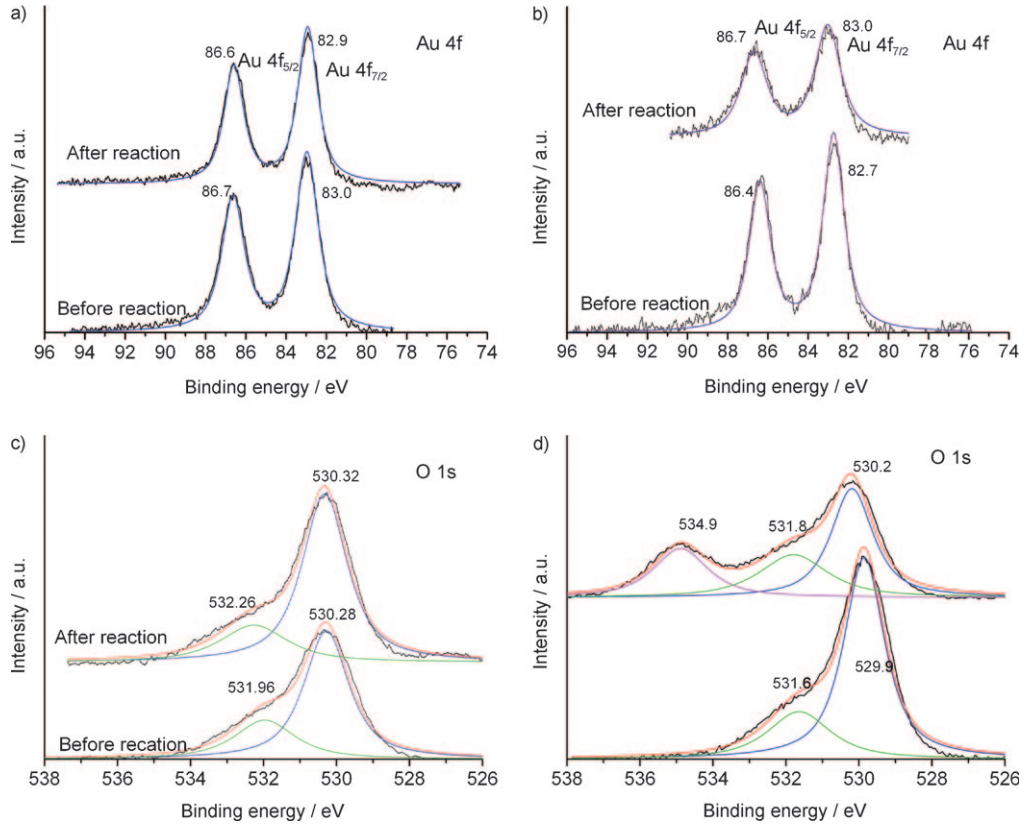

Figure 5. XPS spectra of Au 4f and O 1s for a) and c) Au/NTM and b) and d) Au/NTA catalysts before and after catalytic oxidation of CO.

strates showed negligible activity under the same conditions, there is no doubt that the enhanced activity was due to the presence of Au-NPs. We note that when using other metal oxide supports with large band gaps (e.g., ZrO_2, CeO_2), Au-NPs also exhibit high activity.[4] It has been reported that the Au/TiO_2 photocatalysts have high activity for the oxidation of organic molecules,[25] but the role of the Au-NPs has not been correctly explained because the photocatalytic activity of the Au-NPs themselves under visible light has not been recognized. The results of the present study provide clues to understanding these issues better. Clearly, it is the Au-NPs, rather than the semiconductor TiO_2 supports, that act as the active photocatalyst under visible light irradiation. The visible light absorbed by the Au-NPs due to the surface plasmon resonance (SPR) effect[4] should be able to induce transition of the 6 sp electrons of gold to high energy levels. These energetic electrons can then migrate to the conduction band of TiO_2 and are seized by the oxygen molecules.[31] Meanwhile, Au-NPs can capture electrons from the HCHO molecules adsorbed on them because of the high electronegativity of gold. O_2 adsorbed on the TiO_2 supports surface should be the major electron acceptor (the oxidant). The more O_2 adsorbed, the higher the oxidation activity. Because the surface OH groups and adsorbed H_2O can facilitate O_2 adsorption on the surface and enhance oxygen mobility on the supports,[30] the ability to regain surface OH groups and H_2O can thus act as an indicator for the O_2 adsorption as well as for the oxidation activity. These steps are illustrated in Figure 7.

The roles of the surface OH groups in the catalytic oxidations: In the low-temperature CO oxidation, the observed Au/TiO_2 catalyst activity follows the same order as in the photocatalytic oxidation of HCHO (Table 1). This is logical because the supports serve as an oxygen reservoir and provide oxygen for the CO oxidation on the catalyst. DFT calculations by Hu et al.[16] showed that molecular O_2 cannot absorb on a perfect TiO_2 surface, but instead can only absorb on oxygen vacancies. The surface OH groups could facilitate the absorption of molecular O_2 by donating electrons to TiO_2, and these excess electrons could be delocalized among the Ti atoms that act as the active sites to absorb molecular O_2. In addition, as reported by Kung et al.,[9] the surface OH groups or moisture can remove surface carbonate species, which are the reaction intermediates in the CO oxidation and can block the active sites. Clearly, the existence of surface OH groups is important in the CO oxidation reaction because they directly contribute to the supply of active oxygen species and the regeneration of the active sites in the reaction.

Similar to the above two reactions, in the photocatalytic decomposition of SRB on the bare TiO_2 nanostructures under UV light irradiation (300–400 nm), the observed photoactivity order of the TiO_2 nanostructures was consistent

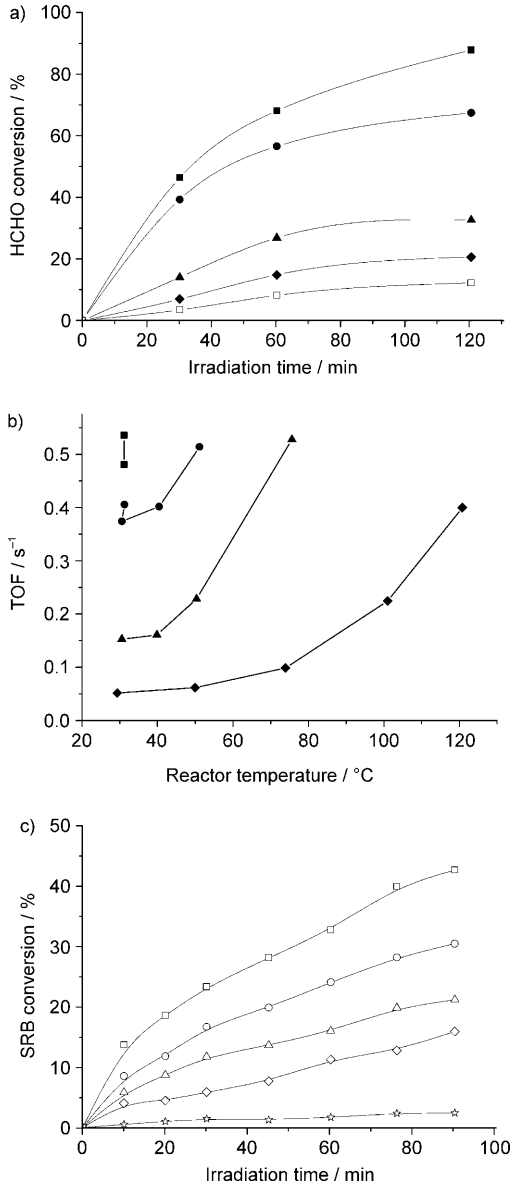

Figure 6. a) Activity performance for the oxidization of HCHO at 20°C under blue light illumination; b) specific activity at 197.8 mL min^{-1} of Au catalysts supported on various TiO_2 nanostructures; c) photocatalytic activity for the decomposition of SRB on bare TiO_2 nanostructured photocatalysts under UV irradiation (■ = Au/NTA, ● = Au/NTBA, ▲ = Au/NTMA, ◆ = Au/NTM, □ = NTM, ○ = NTBA, △ = NTMA, ◇ = NTM, ☆ = blank).

with that of the ability to regain surface OH groups and absorbed water. According to the literature, in this reaction an O_2 molecule seizes a photogenerated electron in the conduction band of TiO_2 to form the superoxide anion ($O_2^{\bullet-}$) species, which then reacts with protons to yield H_2O_2 and H_2O. The photogenerated holes lead to the formation of OH radicals that have a strong oxidation ability to decompose organic molecules. The relevant equations [Eq. (1)–(5)] are summarized below (in which h^+ stands for a photoexcited hole, R represents an organic molecule, and −OH is the surface OH group):[1,32]

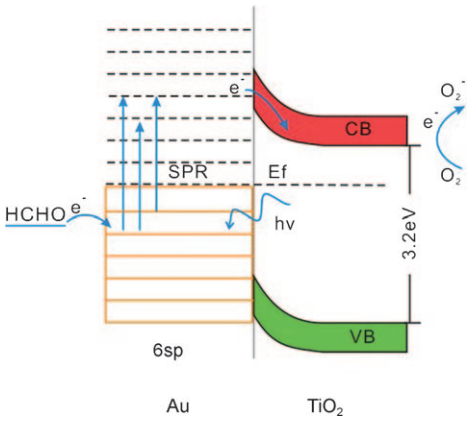

Figure 7. Energy diagram of Au/TiO_2 catalysts showing the oxidation of HCHO by the SPR effect of Au-NPs under visible light.

$$TiO_2 + h\nu(\geq E_g) \rightarrow e^- + h^+ \quad (1)$$

$$h^+ + -OH \rightarrow OH^{\bullet} \quad (2)$$

$$OH^{\bullet} + R \rightarrow CO_2 + H_2O \quad (3)$$

$$e^- + O_2 \rightarrow O_2^{\bullet-} \quad (4)$$

$$e^- + h^+ \rightarrow \text{heat} \quad (5)$$

The formation of $O_2^{\bullet-}$ species consumes photogenerated electrons, preventing them from recombination with the holes so that the reaction rate depends on the formation of $O_2^{\bullet-}$ species and hydroxyl radicals, and thus O_2 molecule adsorption on the TiO_2 surface is of essential importance for the reaction.

Structural model for the regeneration of surface OH and active oxygen species: The catalysis results demonstrate that the activities of the photocatalysts and the catalysts for the three catalytic oxidations rely on the ability of the TiO_2 nanostructures to regain surface OH groups and absorbed water. As previously mentioned, this and the O_2 adsorption ability arise from surface defects. To reveal the structure of these important sites, we determined the outer surface plane of anatase nanostructures (NTA) from the HRTEM image (see Figure S2 in the Supporting Information). The two interplanar spacings were both measured as 0.36 nm, which is in agreement with (010) and (100) (0.378 nm according to JCPDS 71-1166). The angle between the two indicated planes is 90°. Therefore, the two planes can be indexed as the (010) and (100) plane, respectively, and the surfaces most probably exposed are the (001) and (101) planes.

According to a density functional theory (DFT) calculation by Grätzel et al., water is preferably dissociated on the bridging oxygen vacancies on the (101) and (001) surfaces of anatase to form two OH bridging groups,[13] and these OH groups can lower the O_2 adsorption energy further to facilitate molecular O_2 adsorption,[16,17] resulting in molecular O_2 adsorption over the two Ti atoms near the OH group. By combining the literature results with the results from the

present study, we can propose a structural model to illustrate the absorption of H_2O and O_2 molecules on the anatase (001) plane (Figure 8). According to this model, both the absorption and the activation of molecular O_2 are related to the surface oxygen vacancy density and distribution. Therefore, it can easily explain the experimental facts as to why the supported gold catalyst on reducible oxides are more active towards CO oxidation than that on nonreducible oxides,[33] that is, it is easier to generate oxygen vacancies on reducible oxides and these supports can adsorb O_2 molecules, whereas it is generally impossible for nonreducible oxides. The activated oxygen species can directly participate in the oxidation reactions. For supported gold catalysts it has also been suggested that oxygen can be activated on nanoparticles and then react with hydroxyl groups on a support.[9,21] Even in such a mechanism, molecular O_2 activated on the TiO_2 surface provides an additional oxidation agent, and thus enhances oxidation together with the regenerated surface hydroxyl groups. Loading Au-NPs on the TiO_2 supports is likely to create more defects on the interface between the gold particles and the support, which can act as active sites.[12] Therefore, the supports for the gold catalysts not only act as the substrates that allow gold to be adequately dispersed as small Au-NPs, but also play a crucial role in the adsorption of O_2 and the supply of active oxygen for catalytic oxidation.

For the three reactions investigated in this study, the ability to adsorb and activate O_2 molecules, the oxidant in these oxidation reactions, is the most significant factor contributing to the catalytic activity. This ability depends on the oxygen vacancies on the TiO_2 surface. Because surface OH vibration bands of different samples (with different TiO_2 phase composition) appear at the same position, it is most likely that the structure of the vacancy sites in different samples is similar and is located at bridging O^{2-} sites. Therefore, the more O vacancy sites there are, the easier it is to regenerate surface OH groups and to activate the molecular O_2, and the higher the activity of TiO_2-based catalysts and photocatalysts for the oxidations.

We noted that the NTA sample possessed the smallest specific surface area among the four samples but exhibited the strongest ability to form surface OH groups and absorb water. The oxygen vacancy density on the anatase surface is probably higher than that on the surface of the other TiO_2 polymorphs, thus a higher activity is observed from the catalysts of anatase solid. Because the surface OH regeneration ability can act as an indicator of the ability to activate molecular oxygen, we can probably avoid the need to measure the short-lived surface oxygen species in many catalytic studies on supported Au catalysts. Furthermore, in the low-temperature oxidation of CO on gold catalysts, because it is the molecular O_2 and not the lattice oxygen of the catalyst supports that are involved in the oxidation reaction, we can understand further why the mobility of the lattice oxygen is not directly related to their catalytic performances.

Conclusion

Four kinds of TiO_2 nanostructures with different phase compositions, namely, NTM, NTMA, NTBA, and NTA, and their supported Au catalysts have been prepared and used for the three catalytic oxidation reactions. It was found that the order of the catalytic activity of the catalysts in the three reactions are the same as that of the surface OH regeneration ability of the catalyst supports, NTA > NTBA > NTMA > NTM. This observation reveals the common nature of these three catalytic oxidation reactions: the surface OH groups of the catalyst supports contribute to the three reactions, especially the adsorption and activation steps of the O_2 molecules. XPS measurements have identified one O 1s peak at 534.9 eV on Au/TiO_2 (NTA) after its exposure to CO gas, revealing the strong interaction between the coexisting CO and OH species on this catalyst and the abundance of OH groups on the NTA support. This peak should be assigned to the hydroxycarbonyl-like species, an intermediate proposed by Kung et al. A structural model for the generation of surface OH groups and absorption of

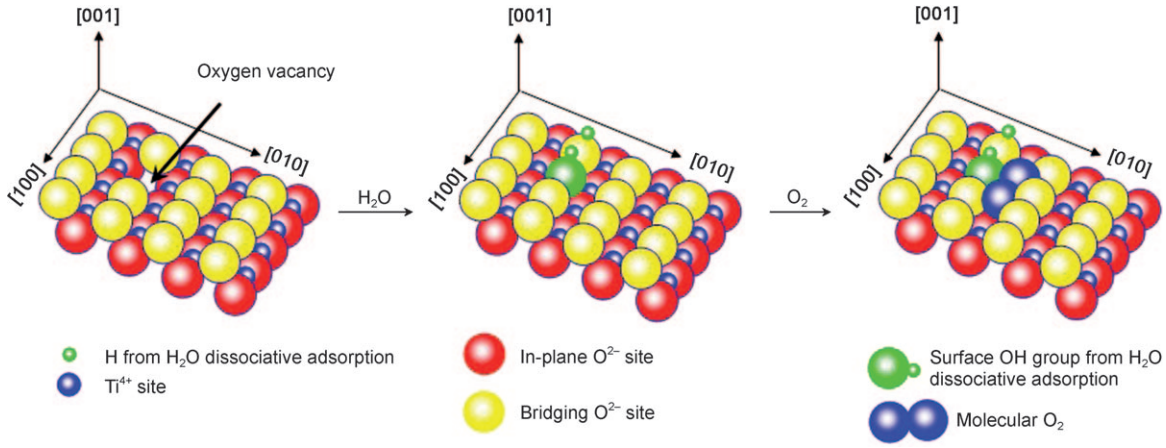

Figure 8. Proposed H_2O and O_2 adsorption process on exposure of the (001) plane in anatase.

molecular oxygen based on the structural characterization and literature results is thus proposed: The oxygen vacancies at the bridging O^{2-} sites of the TiO_2 surface can readily and dissociatively absorb H_2O molecules to generate surface OH groups, which facilitate adsorption and activation of O_2 molecules bound to nearby oxygen vacancies. This O_2 activation step is the key step of the three oxidation reactions. A mechanism for the photocatalytic formaldehyde decomposition on the Au–TiO_2 catalysts is also proposed, which is different from those previously reported in the literature: The Au-NPs can absorb visible light owing to the surface plasmon resonance effect, thus inducing a transition of the 6 sp electrons of gold to high energy levels. These energetic electrons can then migrate to the conduction band of TiO_2 and are seized by the oxygen molecules. Meanwhile, the Au-NPs capture electrons from the formaldehyde molecules adsorbed on them because of their high electronegativity. O_2 adsorbed on the TiO_2 supports surface thus acts as the major electron acceptor. The knowledge acquired in this study will be useful in designing efficient catalysts and photocatalysts for a number of oxidation reactions and for understanding their working mechanisms.

Experimental Section

Synthesis of TiO_2 nanotubes and nanorods and Au loading: Titania nanotubes and nanorods of different phase compositions (labeled as NTM, NTMA, NTBA, and NTA) were prepared through various post treatments of hydrogen titanate nanotubes at temperatures ranging from 300 to 400 °C in different gases. The hydrogen titanate nanotubes were obtained by a hydrothermal treatment of anatase powder with NaOH solution (10 M) and subsequent ion exchange with H^+.[34] NTM and NTBA were obtained after calcination of the hydrogen titanate nanotubes at 300 and 350 °C, respectively, in air for 3 h, whereas NTA was obtained after calcination at 400 °C in argon gas for 3 h. NTMA was obtained by first treating the hydrogen titanate nanotubes with a HNO_3 (0.1 M) solution in a water bath at 60 °C for 12 h, and was then washed with deionized (DI) water and dried at 100 °C overnight before calcination at 300 °C in air for 3 h. After the various treatments, NTM were nanotubes of a metastable phase between the hydrogen titanate and TiO_2(B) phase, whereas NTBA were nanotubes of mixed TiO_2(B) and anatase phases. NTA consisted of nanorods of the anatase phase, and NTMA was composed of the metastable phase nanotubes covered with a thin layer of anatase. The Au-NPs were prepared by a sonication-assisted reduction method that employed $HAuCl_4$ as the precursor, lysine as the capping agent, and $NaBH_4$ as the reduction reagent.[35] In a typical preparation of a Au/TiO_2 catalyst (3 wt%) and DI water (8 mL) were added to the nanotube support (0.50 g), followed by addition of $HAuCl_4$ (0.01 M, 8 mL) and an aqueous solution of lysine (0.01 M, 9 mL). The pH value of the suspension was then adjusted to a value between 5 and 5.5 by using NaOH solution (0.10 M). Thereafter, the suspension was subjected to ultrasonication for 20 seconds. Freshly prepared $NaBH_4$ (0.1 M, 5–10 times the Au molar number) was injected during sonication. After the reaction, the pH value at the end point was measured. The suspension was then washed four times with DI water and centrifugation was carried out before drying at 60 °C overnight and calcining at 300 °C for 1 h. This method can lead to a nearly complete gold precipitation from the gold precursor solution as proven in our previous report.[36]

Catalytic activity test—HCHO oxidation: The Au/TiO_2 catalysts (20 mg) were suspended in ethanol (0.5 mL) to coat the solid onto a glass plate (7 cm in diameter), which was then dried at 80 °C. The coated plate was placed in a 6 L glass vessel located in a chamber equipped with six 18 W light tubes (Philips, TLD18, wavelength 400–500 nm) as the light source. The chamber temperature was actively maintained at 20 °C, otherwise the light illumination could cause an increase in the temperature of the vessel. The vessel was filled with air and sealed after the coated glass plate was mounted. Formaldehyde (4 μL, 40% solution) was injected into the vessel and allowed to fully evaporate with the help of an internal fan. The gaseous specimens were sampled before and after the light was switched on, and were analyzed by a gas chromatograph (Shimadzu GC-2014) equipped with TCD and FID detector.

CO oxidation: The measurement of the catalytic activity for CO oxidation was carried out in a fixed-bed microreactor. Each catalyst (10 mg) was loaded in the middle of a quartz tube in between two layers of quartz wool. Prior to the characterization and activity test, the catalyst was first treated in air at 300 °C for 1 h to remove the lysine molecules that capped the Au particles. After cooling to room temperature, a reactant gas containing CO (1%) in air was then passed through the catalyst bed. The outlet gas was analyzed on-line by using gas chromatography (Shimadzu-14B). Each catalyst was tested at two gas hourly space velocities (GHSV) of 47771 h^{-1} and 472452 h^{-1}.

SRB oxidation: In this study, the UV light source for the photoactivity test was six 20 W tubular Hg lamps (NEC, FL20SBL) with a peak wavelength at about 350 nm. The catalyst concentration was 0.5 g/L, and the initial concentration (C_0) of the SRB (Aldrich) was 1.8×10^{-5} M. At regular irradiation time intervals, the dispersion was sampled, and the specimen was filtered through a filter (Millipore, 400 nm, teflon) to remove the catalyst particles prior to the analysis. The filtrate was analyzed by UV/VIS spectroscopy (Varian Cary 100 spectrometer) for the absorbance intensity by using the reading at 565 nm.

Characterization techniques: The TEM study on the samples and the HRTEM investigations were carried out on a FEI Tecnai F20 operating at 200 kV. XRD patterns of the samples were recorded on a Philips PANalytical X'Pert PRO diffractometer using $Cu_{K\alpha}$ radiation ($\lambda = 1.5418$ Å) operating at 40 kV and 40 mA with a fixed slit. The Raman spectra of the samples were measured on a Spectra-Physics model 127, the excitation source was a He–Ne laser (633 nm) and the resolution was 2 cm^{-1}. The Au loadings in the catalysts were measured on an X-ray fluorescence spectrometer (Bruker Axs, S4 Explorer), and the nitrogen sorption isotherms were measured by the volumetric method on an automatic adsorption instrument (Micromeritics, Tristar 3000) at liquid nitrogen temperature (77 K). The specific surface area was calculated by the BET method from the data in a P/P_0 range between 0.05 and 0.2. The XPS data were recorded on an ESCALAB 250 spectrometer and $Al_{K\alpha}$ radiation was used as the X-ray source. The C 1s peak at 284.5 eV was used as a reference for the calibration of the binding energy scale. The IES measurements were carried out on a Digilab FTS-60A spectrometer equipped with a TGS detector, which was modified by replacing the IR source with an emission cell (the principles of the emission experiment have been published elsewhere).[37] The same amount (in volume) of powder for different samples was loaded on the sample holder to form a uniform thin layer. During the IES measurement, the specimen was heated from 100 to 300 °C and then cooled from 300 to 100 °C on a sample holder at 50 °C intervals in a flow of N_2 (15 standard cubic centimeters per minute deliberately controlled with a flow meter) in an closed but not sealed chamber to remove desorbed species from the specimen. The interval between the two scans (while the temperature was raised to the next hold point) was approximately 120 s for the powdered sample to reach temperature equilibrium. When the specimen was heated, the species adsorbed on the surface such as adsorbed water and OH groups were gradually removed. The extent of the removal varied from sample to sample, depending on the adsorption strength of the species on the sample surface. The maximum heating temperature was limited at 300 °C to prevent the specimen from undergoing a phase change. When the specimen at 300 °C was cooled, trace moisture in the N_2 flow resulted in adsorption of water and the formation of surface OH groups. Similarly, the extent of the adsorption and the formation depended on the strength of the interaction between the species and the sample surface. By comparing the water desorption and the loss of the surface hydroxyl groups during heating with water adsorption and the gain of the surface hydroxyl groups

during cooling, the ability of the surface to generate surface OH groups and to adsorb water was determined. The IES measurement was repeated and the data were well reproducible. The IES spectra at the lower temperatures always contained more noise owing to the low signal-to-noise ratio caused by the low temperature difference between the sample and the detector.

Acknowledgements

Financial Support from the Australian Research Council (ARC) is gratefully acknowledged. Z.Z. thanks the Agency for Science Technology and Research (A-Star) for financial support, as well as Drs. P. K. Wong, Armando Borgna, and Keith Carpenter for their kind support of this collaboration.

[1] A. L. Linsebigler, G. Q. Lu, J. T. Yates, *Chem. Rev.* **1995**, *95*, 735–758.
[2] T. L. Thompson, J. T. Yates, *Chem. Rev.* **2006**, *106*, 4428–4453.
[3] B. Veyret, R. Lesclaux, M. T. Rayez, J. C. Rayez, R. A. Cox, G. K. Moortgat, *J. Phys. Chem.* **1989**, *93*, 2368–2374.
[4] X. Chen, H. Y. Zhu, J. C. Zhao, Z. F. Zheng, X. P. Gao, *Angew. Chem.* **2008**, *120*, 5433–5436; *Angew. Chem. Int. Ed.* **2008**, *47*, 5353–5356.
[5] M. Haruta, N. Yamada, T. Kobayashi, S. Iijima, *J. Catal.* **1989**, *115*, 301–309.
[6] M. S. Chen, D. W. Goodman, *Science* **2004**, *306*, 252–255.
[7] K. I. Hadjiivanov, D. G. Klissurski, *Chem. Soc. Rev.* **1996**, *25*, 61–69.
[8] E. Wahlstrom, E. K. Vestergaard, R. Schaub, A. Ronnau, M. Vestergaard, E. Laegsgaard, I. Stensgaard, F. Besenbacher, *Science* **2004**, *303*, 511–513.
[9] M. C. Kung, R. J. Davis, H. H. Kung, *J. Phys. Chem. C* **2007**, *111*, 11767–11775.
[10] G. C. Bond, D. T. Thompson, *Gold Bull.* **2000**, *33*, 41–51.
[11] C. K. Costello, J. H. Yang, H. Y. Law, Y. Wang, J. N. Lin, L. D. Marks, M. C. Kung, H. H. Kung, *Appl. Catal. A* **2003**, *243*, 15–24.
[12] M. Daté, M. Okumura, S. Tsubota, M. Haruta, *Angew. Chem.* **2004**, *116*, 2181–2184; *Angew. Chem. Int. Ed.* **2004**, *43*, 2129–2132.
[13] A. Vittadini, A. Selloni, F. P. Rotzinger, M. Grätzel, *Phys. Rev. Lett.* **1998**, *81*, 2954–2957.
[14] D. J. C. Yates, *J. Phys. Chem.* **1961**, *65*, 746–753.
[15] P. Jackson, G. D. Parfitt, *Trans. Faraday Soc.* **1971**, *67*, 2469–2483.
[16] L. M. Liu, B. McAllister, H. Q. Ye, P. Hu, *J. Am. Chem. Soc.* **2006**, *128*, 4017–4022.
[17] M. A. Henderson, W. S. Epling, C. H. F. Peden, C. L. Perkins, *J. Phys. Chem. B* **2003**, *107*, 534–545.
[18] Z. Y. Zhong, J. Highfield, M. Lin, J. Teo, Y. F. Han, *Langmuir* **2008**, *24*, 8576–8582.
[19] R. Coquet, K. L. Howard, D. J. Willock, *Chem. Soc. Rev.* **2008**, *37*, 2046–2076.
[20] J. A. van Bokhoven, C. Louis, J. T Miller, M. Tromp, O. V. Safonova, P. Glatzel, *Angew. Chem.* **2006**, *118*, 4767–4770; *Angew. Chem. Int. Ed.* **2006**, *45*, 4651–4654.
[21] J. D. Henao, T. Caputo, J. H. Yang, M. C. Kung, H. H. Kung, *J. Phys. Chem. B* **2006**, *110*, 8689–8700.
[22] M. Haruta, *Nature* **2005**, *437*, 1098–1099.
[23] I. M. Arabatzis, T. Stergiopoulos, D. Andreeva, S. Kitova, S. G. Neophytides, P. Falaras, *J. Catal.* **2003**, *220*, 127–135.
[24] R. S. Sonawane, M. K. Dongare, *J. Mol. Catal. A* **2006**, *243*, 68–76.
[25] L. Armelao, D. Barreca, G. Bottaro, A. Gasparotto, C. Maccato, C. Maragno, E. Tondello, U. L. Stangar, M. Bergant, D. Mahne, *Nanotechnology* **2007**, *18*.
[26] M. A. Cortes-Jacome, G. Ferrat-Torres, L. F. F. Ortiz, C. Angeles-Chavez, E. Lopez-Salinas, J. Escobar, M. L. Mosqueira, J. A. Toledo-Antonio, *Catal. Today* **2007**, *126*, 248–255.
[27] M. Primet, P. Pichat, M. Mathieu, *J. Phys. Chem.* **1971**, *75*, 1216–1226.
[28] O. Takahashi, S. Yamanouchi, K. Yamamoto, K. Tabayashi, *Chem. Phys. Lett.* **2006**, *419*, 501–505.
[29] D. A. H. Cunningham, W. Vogel, M. Haruta, *Catal. Lett.* **1999**, *63*, 43–47.
[30] A. Bongiorno, U. Landman, *Phys. Rev. Lett.* **2005**, *95*, 106102.
[31] Y. Tian, T. Tatsuma, *J. Am. Chem. Soc.* **2005**, *127*, 7632–7637.
[32] C. S. Turchi, D. F. Ollis, *J. Catal.* **1990**, *122*, 178–192.
[33] M. M. Schubert, S. Hackenberg, A. C. van Veen, M. Muhler, V. Plzak, R. J. Behm, *J. Catal.* **2001**, *197*, 113–122.
[34] Y. Lan, X. P. Gao, H. Y. Zhu, Z. F. Zheng, T. Y. Yan, F. Wu, S. P. Ringer, D. Y. Song, *Adv. Funct. Mater.* **2005**, *15*, 1310–1318.
[35] Z. Zhong, J. Ho, J. Teo, S. Shen, A. Gedanken, *Chem. Mater.* **2007**, *19*, 4776–4782.
[36] Z. Y. Zhong, J. Y. Lin, S. P. Teh, J. Teo, F. M. Dautzenberg, *Adv. Funct. Mater.* **2007**, *17*, 1402–1408.
[37] R. L. Frost, A. M. Vassallo, *Clay Miner.* **1996**, *44*, 635–651.

Received: June 12, 2009
Published online: November 13, 2009

